Journal of Colloid and Interface Science 544 (2019) 241–248

Contents lists available at ScienceDirect

Journal of Colloid and Interface Science

journal homepage: www.elsevier.com/locate/jcis

Regular Article

# Nanoporous carbon spheres derived from metal-phenolic coordination polymers for supercapacitor and biosensor

Gen Wang, Jing Qin, Yongxi Zhao, Jing Wei *

*The Key Laboratory of Biomedical Information Engineering of Ministry of Education, School of Life Science and Technology, Xi'an Jiaotong University, Xi'an, Shaanxi 710049, China*

## GRAPHICAL ABSTRACT

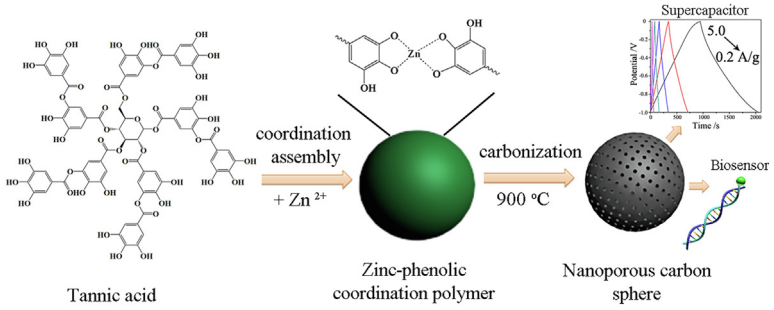


## ARTICLE INFO

*Article history:*
Received 22 September 2018
Revised 28 February 2019
Accepted 1 March 2019
Available online 2 March 2019

*Keywords:*
Mesoporous material
Carbon
Coordination polymer
Sensor
Supercapacitor

## ABSTRACT

The conversion of plant polyphenol to multi-functional nanoporous carbon spheres (NCSs) is desirable and challenging. Tannic acid (TA), as one kind of plant polyphenol, has been regarded as one of potential renewable carbon sources for nanoporous carbon materials. However, the nanoporous carbon materials derived from TA usually show low surface area and irregular morphology, which partially limit their broad applications. Herein, we demonstrate the successful synthesis of NCSs with high surface area (up to 2221 $m^2/g$) and uniform diameter (~120 nm) by direct carbonization of zinc-phenolic coordination polymer using TA as a carbon source. The zinc contents play an important role in tailoring the porosity of NCSs. The specific surface area of NCSs can be adjusted in the range of 527–2221 $m^2/g$ as the zinc contents in the coordination polymers changed from 0 to 8.6 wt%. To verify the multi-functions of NCSs, such carbon spheres are further used as a sensing platform for the analysis of nucleic acid variants with high selectivity and low limit of detection, and electrode material for supercapacitor with high specific capacitance, good capacitance retention, and excellent cyclic stability.



## 1. Introduction

Nanoporous carbon spheres (NCSs) have attracted intensive interests due to their high surface area, good conductivity and various applications in catalysis, adsorption, drug delivery, environmental remediation, as well as energy conversion and storage [1–5]. Many attempts have been made to synthesize NCSs with unique structure, tunable diameter and pore size, as well as heteroatoms doping to tailor the physicochemical property of carbon spheres. Till now, different synthetic methods such as soft and hard templating [6–9], self-assembly [10], emulsion polymerization [11], sol-gel process [12–14] and hydrothermal carbonization [15,16] have been developed to tailor the porosity, nanostructure and compositions of the NCSs. As the carbon source can affect the textural properties of the derived carbon spheres [17–18], it

* Corresponding author.
*E-mail address:* jingwei@xjtu.edu.cn (J. Wei).

https://doi.org/10.1016/j.jcis.2019.03.001
0021-9797/

is still challenging but desirable to explore new carbon source that features highly abundance, low cost, nontoxicity, high thermal stability and easy functionalization to realize controllable and sustainable synthesis of NCSs for various applications. Biomass has been regarded as a very promising carbon source to synthesize NCSs [19–26]. For example, glucose, fructose and sucrose have been used to synthesize carbon spheres via a hydrothermal carbonization process. However, the carbon spheres synthesized by hydrothermal carbonization of biomass usually showed microporous structure with small pore size, which hinder their wide applications involving large-sized guest molecules or fast mass transport [2].

Recently, metal-organic frameworks (MOFs) have been intensively used as a carbon precursor to synthesize nanoporous carbon materials [27–32]. As a typical case, zeolitic imidazolate frameworks-8 (ZIF-8), assembled by Zn ions and imidazole, has been widely used to synthesize N-doped carbon materials with high surface area (up to 3453 $m^2/g$) [33]. Note that most of MOF materials are synthesized using petrochemical products (such as imidazole) as an organic ligand to realize the regular porous structure and crystalline framework. It may be inviable for the large-scale synthesis of nanoporous carbon materials by carbonizing such organic ligands from the point of view of economy and sustainability [34]. It's anticipated that the synthesis of metal-organic coordination polymer spheres using biomass as an alternative organic ligand and transformation of such coordination polymers to nanoporous carbon spheres would be an ideal strategy to synthesize NCSs [35]. However, to the best of our knowledge, very few examples of coordination polymer spheres and their derived nanoporous carbon spheres using biomass as an organic ligand have been reported yet.

Plant polyphenols, extracted from plant tissue, are widely used as a renewable carbon source for the synthesis of nanoporous carbon materials [36–48]. Tannic acid (TA for short), as one kind of plant polyphenols, has plenty of catechol and galloyl groups, which can chelate with different kinds of metal ions to form metal-phenolic coordination polymers [43]. Inspired from the successful synthesis of nanoporous carbon materials from ZIF-8, it is believed that metal-TA coordination polymers would also be a good candidate for carbon materials. Most importantly, the organic ligand (i.e. tannic acid) is a natural product and renewable source. Such synthesis strategy would provide a possibility for sustainable synthesis of nanoporous carbon spheres. For example, we have synthesized crystalline Co-TA coordination polymers and used them as carbon precursors for the synthesis of nanoporous Co/N-C composites, which exhibit super performance for both oxygen reduction reaction and oxygen evolution reaction [45]. Zhang et al. reported the synthesis of ordered mesoporous carbon via a mechanochemical assembly through coordination cross-linking using TA as a carbon precursor, and Zn (or Ni) ions as a crosslinker [46]. Recently, a formaldehyde-assisted metal-ligand crosslinking strategy was developed to synthesize metal-phenolic coordination spheres and their derived carbon composites [47]. However, most of nanoporous carbon derived from TA show low specific surface area (<1000 $m^2/g$) and irregular morphology, which partially limited the broad applications of TA derived carbon materials.

Herein, we demonstrate the successful synthesis of nanoporous carbon spheres with uniform diameter (~120 nm) and high surface area (up to 2221 $m^2/g$) using tannic acid as a sustainable carbon source. The zinc-phenolic coordination polymer spheres (~170 nm) are firstly synthesized via a formaldehyde-assisted metal–ligand crosslinking strategy. Then, the NCSs are obtained by morphology-preserving carbonization of the zinc-phenolic coordination polymers. During the carbonization process, the zinc species can aggregate together to form ZnO nanocrystals, and then be reduced to Zn by carbon. At last, Zn can be fully vaporized from the carbon framework at high temperature, leaving plenty of micropores and mesopores in the carbon spheres. As the contents of zinc species in the coordination polymers can be well adjusted, the porosity and specific surface area of carbon spheres can be easily tailored. Due to the high surface area, micro/mesoporous framework, and uniform spherical morphology, the carbon spheres reveal high specific capacitance (271 F/g), good capacitance retention, and excellent cyclic stability when using as an electrode material for supercapacitor. Furthermore, the carbon spheres can be applied for reliable analysis of nucleic acid variants with single-nucleotide discrimination.

## 2. Results and discussion

Tannic acid has five catechol and five galloyl groups in each molecule (Fig. 1a). Such phenolic groups can chelate with zinc ions in alkaline conditions. The synthesis of NCSs mainly includes two steps (Fig. 1b). In the first step, TA molecules and Zn ions were assembled in the alkaline ethanol/water mixed solvents. In the synthesis process, block copolymers F127 (polyethylene oxide-*block*-polypropylene oxide-*block*-polyethylene oxide, PEO-*b*-PPO-*b*-PEO) were used to stabilize the TA molecules in order to make the polymerization process more controllable. Formaldehyde was used to crosslink the TA molecules to form TA oligomers. Then metal ions (i.e. $Zn^{2+}$) were added into the solution to further crosslink TA oligomers via metal-catechol coordinate bonds. After further hydrothermal treatment at 70 °C, Zn-TA coordination polymer spheres were obtained. In the second step, NCSs were synthesized by controllable carbonization of Zn-TA coordination spheres at 900 °C in nitrogen atmosphere.

The stoichiometric ratio of zinc to organic ligand in the MOF (such as ZIF-8, $Zn(mim)_2$) is fixed due to the crystalline framework and unique chemical structure [49]. Differently, Zn-TA coordination spheres show amorphous structure (Fig. S1a), suggesting the possibility to adjust the content of Zn species in the coordination polymers. During the synthesis process, different amounts of Zn precursor (*i.e.* $Zn(NO_3)_2{\cdot}6H_2O$) were used, and the obtained Zn-TA coordination polymers were denoted Zn-TA-*x* (*x* refers the mass ratio of Zn precursor to TA, *x* = 0, 10, 20, 30, 40, 50 and 60%). After carbonization at 900 °C, the obtained nanoporous carbon spheres were denoted as Zn-TA-*x*-900 (*x* = 0, 10, 20, 30, 40, 50 and 60%).

Scanning electron microscopy (SEM) images for all the Zn-TA-*x* (*x* = 0, 10, 20, 30, 40 and 50%) samples showed spherical morphology with uniform diameter (~170 nm), indicating the successful synthesis of Zn-TA coordination spheres (Figs. 2a–d and S2a and b). When the mass ratio of Zn precursor to TA increased to 60%, the mixtures of coordination spheres and nanoparticles were obtained, suggesting that a higher metal content could lead to the formation of irregular coordination polymers (Fig. S2c). After carbonization, all the coordination polymer spheres were successfully transformed to carbon spheres (Figs. 2e–h and S2d and e), indicating that metal-phenolic coordination polymers were one of excellent precursors to synthesize carbon materials with preserved morphology. Due to the shrinkage of the skeleton, the diameter of the carbon spheres slightly decreased to ~120 nm estimated from the SEM results. Thermalgravimetric analysis (TG) results revealed that the content of zinc in the coordination polymers increased from 1.4 to 8.6 wt% as the mass ratio of Zn precursor to TA increased from 10 to 60 wt% (Fig. S3).

The powder X-ray diffraction (XRD) patterns for Zn-TA-40%-900 displayed two broad peaks at 2θ of 23.5 and 43.6°, corresponding to the diffractions of the amorphous carbon (Fig. S1a). No diffraction peaks were observed for Zn (or ZnO) crystals in the carbon samples, indicating the full vaporization of Zn species during the carbonization process. X-ray photoelectron spectroscopy (XPS)

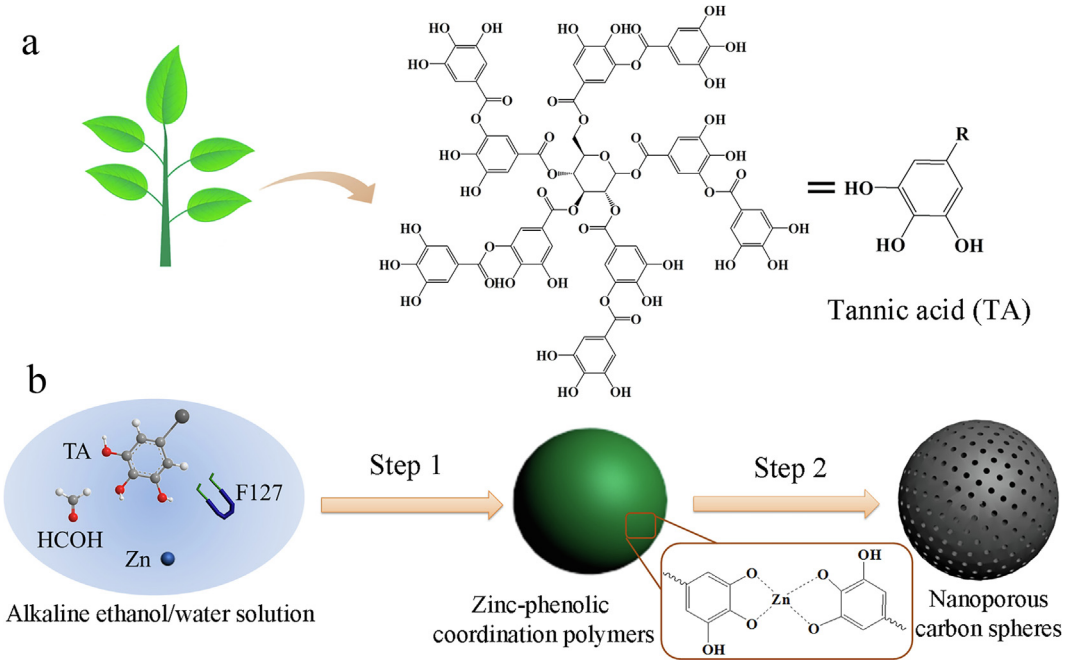


**Fig. 1.** (a) Chemical structure for tannic acid. (b) The schematic synthesis of nanoporous carbon spheres using zinc-phenolic coordination polymers as a carbon source.

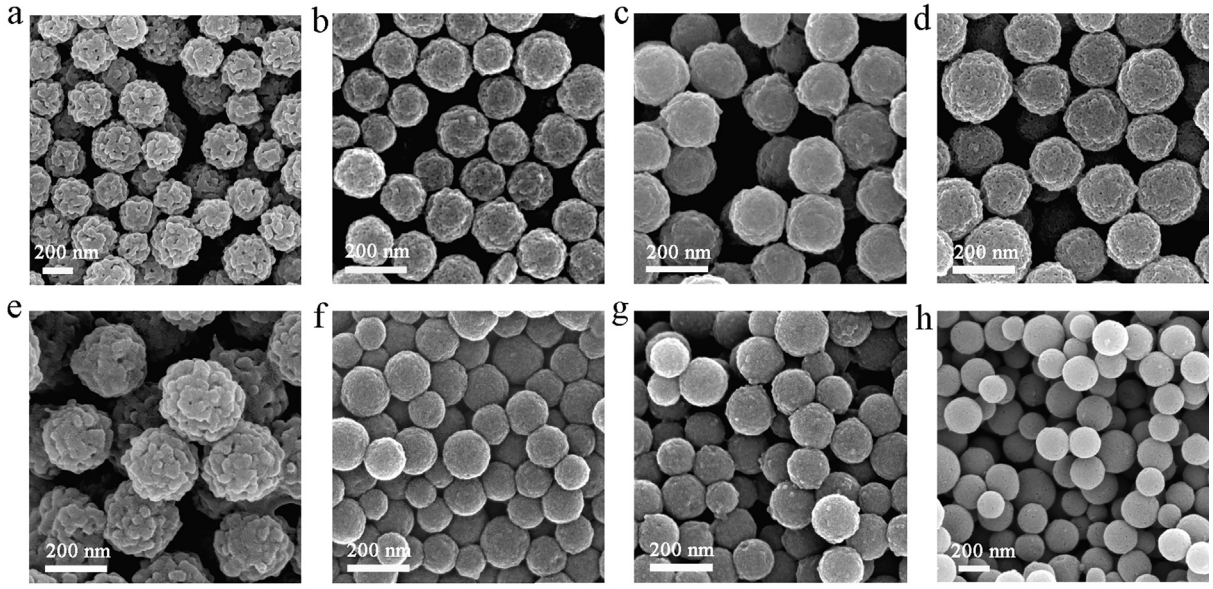


**Fig. 2.** SEM images of Zn-TA coordination polymer spheres and their derived carbon spheres: (a) Zn-TA-0%, (b) Zn-TA-20%, (c) Zn-TA-40%, (d) Zn-TA-50%, (e) Zn-TA-0%-900, (f) Zn-TA-20%-900, (g) Zn-TA-40%-900 and (h) Zn-TA-50%-900.

results also proved the Zn species were fully removed after carbonization at 900 °C (Fig. S4). XPS spectra for Zn-TA-40% reveal the existence of C, N, O and Zn elements. The nitrogen species may be ascribed to the reactions between alkaline ammonium hydroxide and acidic TA during the synthesis process [50]. After carbonization at 900 °C, the peaks for both the N 1s and Zn 2p were not observed from XPS spectra. XPS results proved that N groups were decomposed during the carbonization process. Zn species in the coordination polymers were aggregated together to form ZnO nanoparticles during the carbonization process. At higher temperature, ZnO was reduced by carbon to form Zn metals. Zn metals were vaporized away along with the $N_2$ flow during the carbonization process due to the low boiling point of zinc (~907 °C), resulting in nanoporous framework.

Transmission electron microscope (TEM) techniques were further used to characterize the evolution of Zn species in the carbon framework. The sample Zn-TA-40% was calcined at different temperatures (300–900 °C). The obtained materials were denoted Zn-TA-40%-*y* (*y* = 300, 400, 600 and 900). TEM images for Zn-TA-40%-300 do not reveal any Zn (or ZnO) crystals in the framework (Fig. 3a and b). However, element mapping results prove the zinc species were distributed uniformly in the carbon framework, indicating zinc species show amorphous structure (Fig. S5). The selected area electron diffraction patterns also proved the amorphous structure. When the carbonization temperature increased to 400 °C, the zinc oxide crystals with ultra-small size (<5 nm) were observed in the polymer framework (Figs. 3c, d and S6). As the temperature further increased to 600 °C, it's clearly to see that

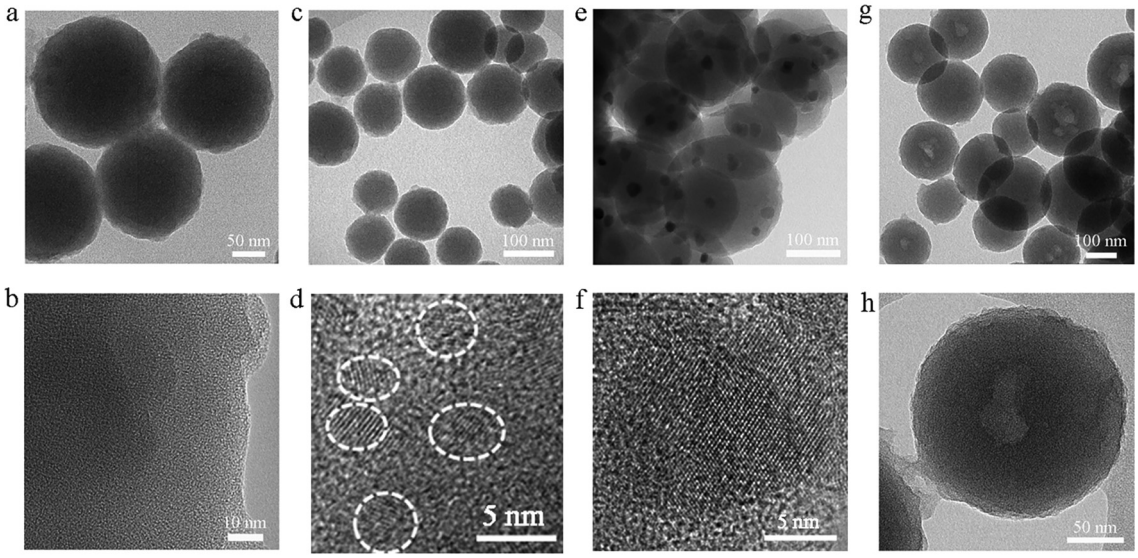


**Fig. 3.** TEM images for Zn-TA-40% carbonized at different temperatures (a and b) 300 °C, (c and d) 400 °C, (e and f) 600 °C, (g and h) 900 °C.

the zinc oxide crystals are embedded in the spherical framework (Fig. 3e). The size of zinc oxide crystals increased dramatically (>10 nm), suggesting a severe aggregation of zinc species during the crystalline process. The high-resolution TEM image for Zn-TA-40%-600 clearly shows the lattice fringes of ZnO, indicating the formation of highly crystalline ZnO particles (Fig. 3f). When the temperature increased to 900 °C, nearly no Zn (or ZnO) crystals were observed, which is consistent to the XPS and XRD results (Fig. 3g and h). Instead, lots of nanopores and cavities were formed in the carbon spheres. Such cavities may be formed as the vaporization of Zn crystals with large crystal size. Raman spectra for Zn-TA-40% carbonized at different temperatures (300–900 °C) revealed that the intensity ratio between G and D bands ($I_G/I_D$) increased gradually as the temperature increased, indicating an enhanced graphitic degree of the carbon materials (Fig. S1b).

The porous structure of NCSs was characterized by $N_2$ sorption isotherms (Fig. 4). $N_2$ sorption isotherms for Zn-TA-0%-900 without using any zinc species exhibited type I curve, indicating a microporous structure. Such results showed that F127 used in the synthesis was not act as a soft template for the production of mesoporous structure. In addition, a large hysteresis loop at a high relative pressure ($P/P_0$, 0.90–0.98) revealed the existence of large pores, which was attributed to the packing of nanospheres. After incorporation of Zn species, $N_2$ sorption isotherms for Zn-TA-$x$-900 ($x$ = 10, 20, 30, 40, 50, 60%) revealed a hysteresis loop at a relative pressure of 0.45, indicating a mesoporous structure. This proved the Zn species could act as a porogen to produce plenty of mesopores in the carbon frameworks.

Brunauer-Emmett-Teller (BET) surface area for the NCSs increased from 527 to 2221 $m^2/g$ as the mass ratio of Zn to TA increased from 0 to 40% (Table 1). The mesoporous surface area also increased from 109 to 774 $m^2/g$ when the mass ratio of Zn to TA increased from 0 to 40%. However, when the mass ratio of Zn to TA further increased from 40 to 60%, BET surface area decreased from 2221 to 713 $m^2/g$. This may be due to the partial collapse of porous structure as large amount of zinc species are vaporized from the carbon framework. The tunable BET and mesoporous surface area for the carbon spheres can be ascribed to the adjustable zinc contents in the coordination polymers. The BET surface area (i.e. 2221 $m^2/g$) of nanoporous carbon spheres prepared in this work is much higher than that of the mesoporous carbon derived from mechanochemical assembly of F127, TA and

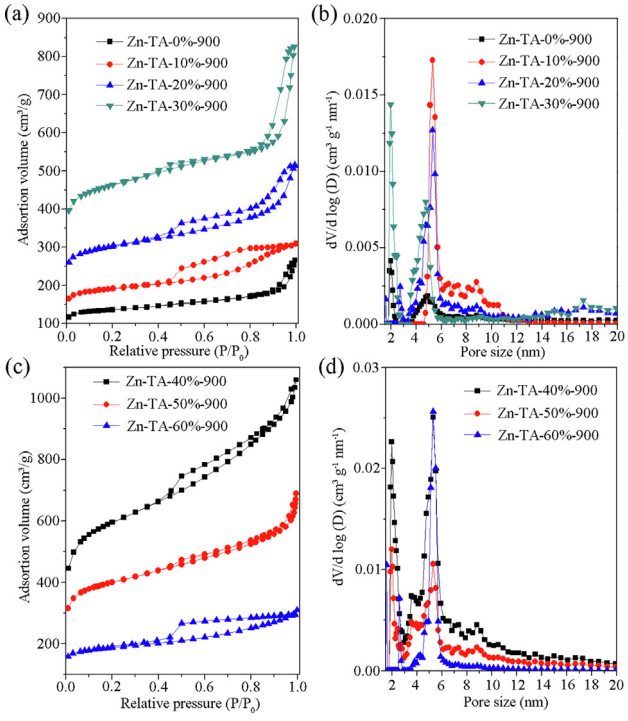


**Fig. 4.** $N_2$ sorption isotherms (a and c) and corresponding DFT pore size distributions (b and d) for Zn-TA-0%-900, Zn-TA-10%-900, Zn-TA-20%-900, Zn-TA-30%-900, Zn-TA-40%-900, Zn-TA-50%-900 and Zn-TA-60%-900 respectively.

metal ions (Zn or Ni) in previous reports (i.e. 395–1057 $m^2/g$) [46]. The nanoporous carbon spheres also showed higher BET surface area than the carbon spheres derived from TA-Co coordination polymers in our previous work (477 $m^2/g$) [47]. The density functional theory (DFT) pore size distributions curves were shown in Fig. 3b and d. The pore size for all the nanoporous carbon spheres was distributed uniformly (4–6 nm). The pore volume for the nanoporous carbon spheres was ranging from 0.41 to 1.64 $cm^3/g$.

Due to the high surface area, micro/mesoporous structure and unique spherical morphology, NCSs were used as an electrode material for supercapacitor. The electrochemical capacitive perfor-

**Table 1**
Textural properties of nanoporous carbons spheres derived from Zn-TA coordination polymers.

| Samples | Zn/TA mol/mol | $S_{BET}$ ($m^2/g$)[a] | $S_{micro}$ ($m^2/g$)[b] | V ($cm^3/g$)[c] | Pore size (nm)[d] |
|---|---|---|---|---|---|
| Zn-TA-0%-900 | 0 | 527 | 418 | 0.41 | 4.9 |
| Zn-TA-10%-900 | 37.4 | 739 | 597 | 0.48 | 5.3 |
| Zn-TA-20%-900 | 74.9 | 1165 | 921 | 0.79 | 5.3 |
| Zn-TA-30%-900 | 112.3 | 1784 | 1423 | 1.27 | 4.7 |
| Zn-TA-40%-900 | 149.8 | 2221 | 1447 | 1.64 | 5.3 |
| Zn-TA-50%-900 | 187.2 | 1521 | 1076 | 1.07 | 5.3 |
| Zn-TA-60%-900 | 224.7 | 713 | 541 | 0.48 | 5.3 |

[a] BET surface area.
[b] Microporous surface area.
[c] Total pore volume.
[d] DFT pore size.

mances were evaluated by cyclic voltammetry (CV) and galvanostatic charge/discharge technique in a three-electrode cell. The CV curves of Zn-TA-40%-900 electrodes in 6 M KOH aqueous electrolyte at varied scan rate from 5 to 200 mV/s showed nearly rectangular shape without any redox peaks, indicating a double-layer capacitance behavior (Fig. 5a). Other carbon spheres derived from Zn-TA coordination polymers with different Zn contents also exhibited similar property (Fig. S7). The charge-discharge tests of Zn-TA-40%-900 electrode were conducted at the current densities from 0.2 to 5.0 A/g (Fig. 5b and c). The specific capacitance for Zn-TA-40%-900 calculated from the charge-discharge curves was 271 F/g at a current density of 0.2 A/g, which was much higher than that for Zn-TA-0%-900 (149 F/g), Zn-TA-10%-900 (169 F/g), Zn-TA-20%-900 (193 F/g), Zn-TA-30%-900 (234 F/g), Zn-TA-50%-900 (201 F/g) and Zn-TA-60%-900 (151 F/g) (Fig. S8). The specific capacitance of Zn-TA-40%-900 can still retain 176 F/g even at a higher current density of 5 A/g. Comparing with other nanoporous carbon spheres prepared using Zn-TA coordination polymers with different zinc contents as a carbon precursor, Zn-TA-40%-900 showed the highest specific capacitance at different current densities due to its high surface area and plenty of mesopores (Figs. 5d and S9b). The specific capacitance for Zn-TA-40%-900 was also comparable to that of other nanoporous carbon materials reported recently (Table S1).

To investigate the electrochemical stability of Zn-TA-40%-900, galvanostatic charge-discharge measurements were performed at

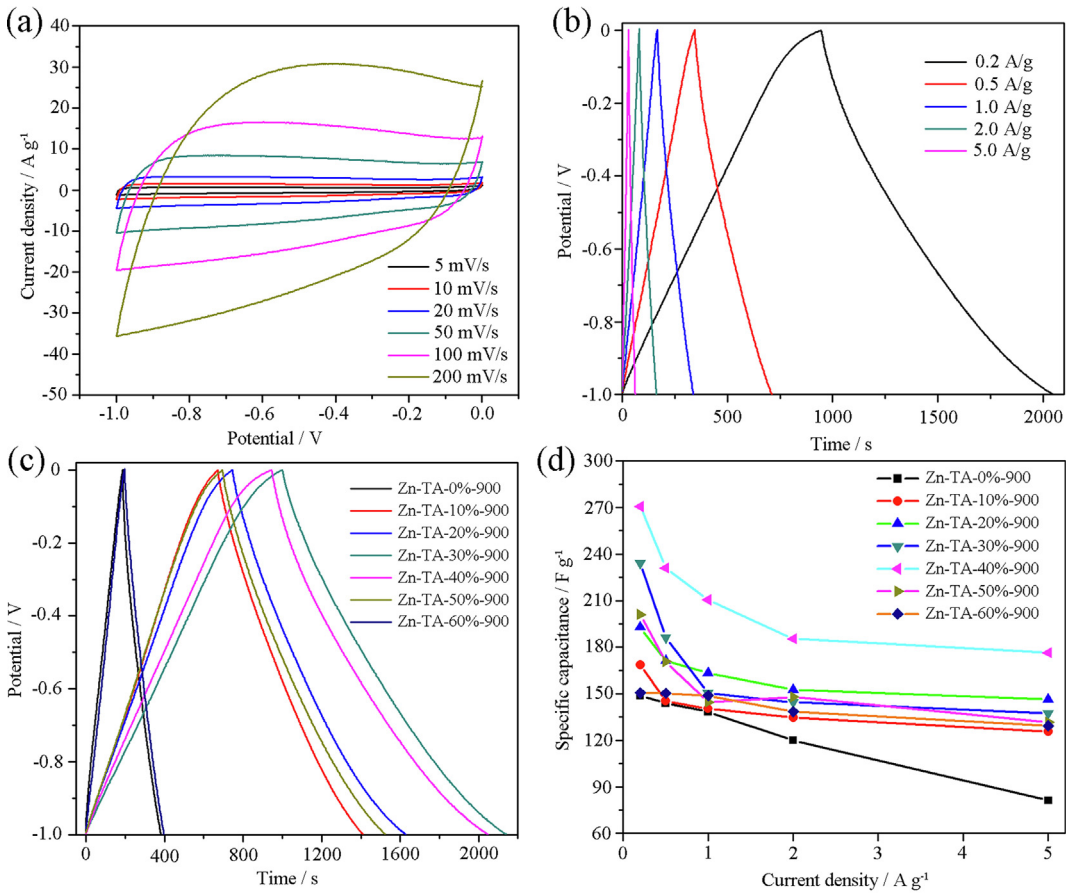


**Fig. 5.** Electrochemical performance of nanoporous carbon spheres derived from the Zn-TA coordination polymers using a three-electrode cell: (a) cyclic voltammograms of Zn-TA-40%-900 at different scan rates (5–200 mV/s) in 6.0 M KOH solution. (b) Galvanostatic charge/discharge curves of Zn-TA-40%-900 at different current densities (0.2–5 A/g). (c) Galvanostatic charge/discharge curves of nanoporous carbon derived from different Zn-TA coordination polymers at a current density of 0.2 A/g. (d) Specific capacitance for carbon spheres at different current densities (0.2–5.0 A/g).

a current density of 5 A/g. The cyclic tests showed that 98% of its initial capacity was maintained after 5000 cycles (Fig. S9a). The NCSs showed unique spherical structure, as well as plenty of micropores and mesopores (4–6 nm) in the carbon framework with total surface area up to 2221 $m^2/g$, which could effectively enhance the ions transport between the different carbon spheres and inside the carbon matrix. As a result, a high specific capacitance has been achieved using such nanoporous carbon spheres as an electrode material.

Carbon nanomaterials have been widely used for fluorescent biosensors due to their high surface area and efficient fluorescence quench ability [51–53]. In this work, NCSs were used as fluorescence sensing platform to detect nucleic acid (Fig. 6a). The NCSs showed higher fluorescence quenching efficiency than Zn-TA coordination polymer spheres (Fig. 6b). Moreover, as the carbonization temperature increased, nanoporous carbon spheres showed enhanced quenching efficiency. The NCSs can adsorb 6-carboxyfluorescein (FAM)-labeled single-strand DNA (ssDNA) through the π-π interactions and quench the fluorescence of FAM-labeled ssDNA. The $sp^2$ hybrid carbon domains in the carbon spheres can bind with ssDNA via π-π interactions [54]. As the carbonization temperature increased, the contents of $sp^2$ hybrid carbon atoms increased evidenced by Raman results (Fig. S1b). Consequently, Zn-TA-40%-900 showed the highest performance for ssDNA adsorption. By comparing the kinetic curves for fluorescence quenching, the carbon spheres showed higher quenching ability than the polymer spheres (Fig. S11a).

Zn-TA-40%-900 was further used as a sensing platform to detect DNA analogue of miRNA-21, because miRNA-21 is one of potential biomarkers in many types of solid tumors [55]. Firstly, FAM-labeled ssDNA probe was designed. Its fluorescence can be quenched by Zn-TA-40%-900. However, the fluorescence was recovered when the target DNA was present (Figs. 6c and S10). This is because a hybridization reaction between FAM-labeled ssDNA

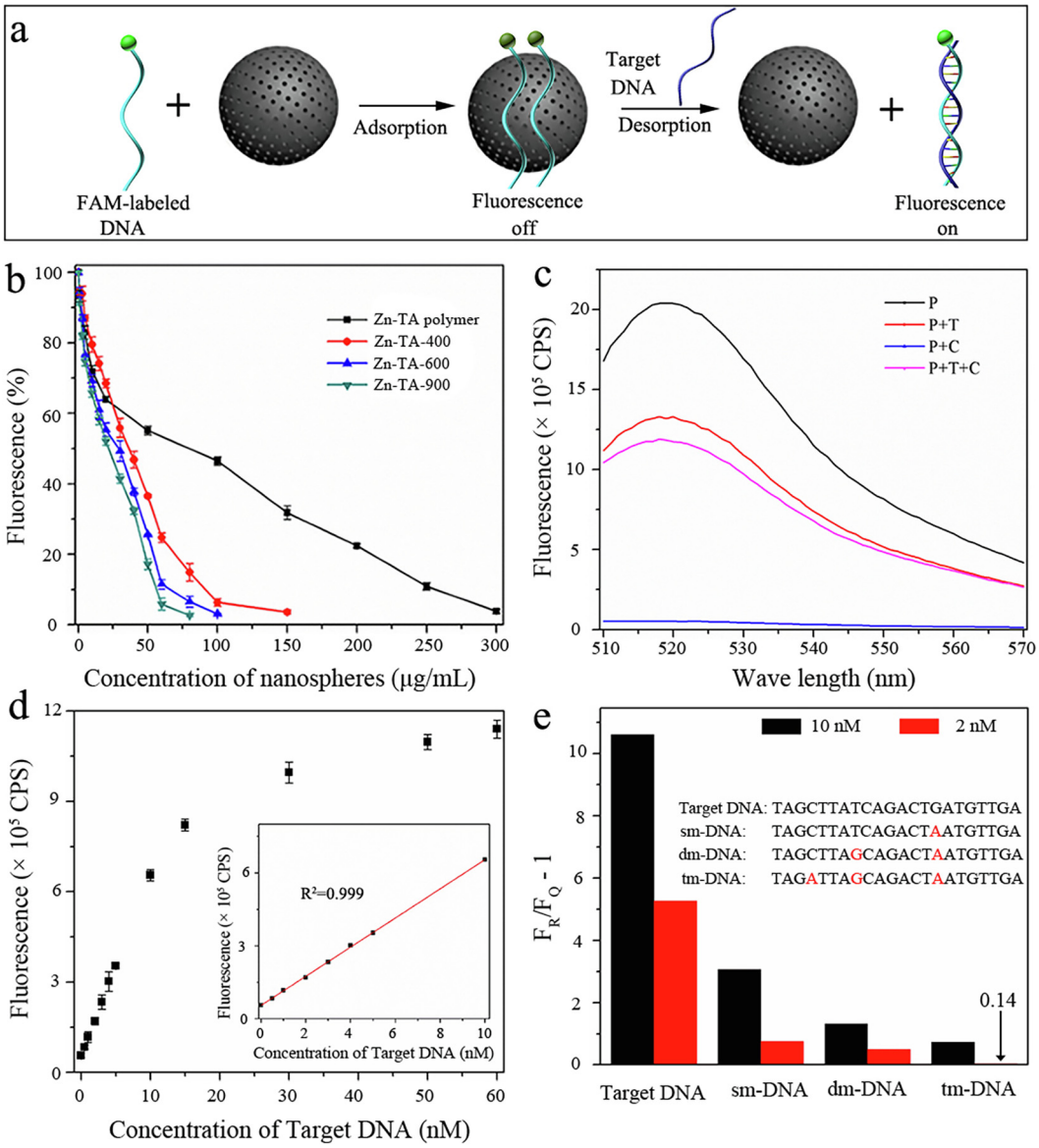


**Fig. 6.** (a) Schematic illustration for the detection of target DNA. (b) Fluorescence intensities of probe DNA at 520 nm versus different concentrations of Zn-TA polymer and carbon spheres. (c) Fluorescence spectra of probe DNA (P, black line); probe DNA and target DNA (P + T, red line); probe DNA and Zn-TA-40%-900 (P + C, blue line); probe DNA, target DNA and Zn-TA-40%-900 (P + T + C, pink line). (d) Fluorescence intensities versus different concentrations of target DNA (0.5–60 nM). Inset is the corresponding calibration curve for target DNA detection. (e) Selectivity for the detection of target DNA. (For interpretation of the references to color in this figure legend, the reader is referred to the web version of this article.)

and target DNA. The formation of double-stranded structure will seal the nitrogenous base and prevent the interactions between carbon and nitrogenous base via π-π stacking. Consequently, the FAM-labeled ssDNA was detached from carbon spheres, resulting into the recovery of fluorescence. By measuring the fluorescence intensity, we can calculate the concentration of target DNA molecules. As shown in Fig. 6d, the fluorescence intensity increased gradually when the concentration of target DNA increased from 0.5 to 60 nM. The curves of fluorescence intensity versus the concentration of target DNA showed a linear relationship in the range of 0.5–10 nM. The detection limit was $0.36 \times 10^{-9}$ M (calculated from 3σ/slope, σ refers standard deviation), which was comparable to that of other sensors fabricated by graphene oxide and carbon nanotube (Table S2). From the kinetic curves of fluorescence recovery, the fluorescence can be recovered for both the polymer and carbon spheres based probe when the target DNA was added. Both carbon and polymer spheres showed that the recovery time was around 1 h. Moreover, the fluorescence recovery efficiency ($F_R/F_Q$ −1, where $F_R$ and $F_Q$ are the fluorescence intensities at 518 nm when target DNA or mismatched sequence of target DNA are present and absent, respectively) of Zn-TA-40%-900 was much higher than that of single-, double- and triple-base mismatched DNA (Fig. 6e), suggesting such nano-probe system had a good selectivity to different nucleic acid molecules and could even distinguish DNA with single nucleotide variation.

## 3. Conclusions

In conclusion, nanoporous carbon spheres with high surface area (up to 2221 $m^2/g$) and unique morphology were synthesized using plant polyphenol as a sustainable carbon source. The zinc-phenolic coordination spheres were firstly synthesized using TA as renewable ligand. After carbonization, the zinc-phenolic coordination spheres were converted to nanoporous carbon sphere with preserved spherical morphology. The nanoporous carbon spheres showed tailorable porosity by simply changing the zinc contents in the zinc-phenolic coordination polymers. Due to the high surface area and unique spherical structure, the nanoporous carbon spheres were used as an electrode material and showed high specific capacitance and a good cyclic stability. The nanoporous carbon spheres could also be used as sensing platforms for the sensitive analysis of nucleic acid variants with single-nucleotide discrimination. This work provides an alternative strategy for the synthesis of nanoporous carbon spheres with high surface area and unique morphology using plant polyphenol as a sustainable carbon source. Moreover, due to the micro/mesoporous structure and high specific surface area, such nanoporous carbon materials will exhibit broad applications such as adsorption and separation, catalysis, sensor and biomedicine.

## Acknowledgements

This work was financially supported by the National Science Foundation of China (No. 21701130), the Fundamental Research Funds for the Central Universities and "Young Talent Support Plan" of Xi'an Jiaotong University. We thank Miss Jiao Li at Instrument Analysis Center of Xi'an Jiaotong University for her assistance with TEM analysis.

## Appendix A. Supplementary material

Supplementary data to this article can be found online at https://doi.org/10.1016/j.jcis.2019.03.001.

## References

[1] A.D. Roberts, X. Li, H. Zhang, Porous carbon spheres and monoliths: morphology control, pore size tuning and their applications as Li-ion battery anode materials, Chem. Soc. Rev. 43 (2014) 4341–4356.
[2] J. Liu, N.P. Wickramaratne, S.-Z. Qiao, M. Jaroniec, Molecular-based design and emerging applications of nanoporous carbon spheres, Nat. Mater. 14 (2015) 763–774.
[3] P. Zhang, Z.-A. Qiao, S. Dai, Recent advances in carbon nanospheres: synthetic routes and applications, Chem. Commun. 51 (2015) 9246–9256.
[4] Y. Zhai, Y. Dou, D. Zhao, P.F. Fulvio, R.T. Mayes, S. Dai, Carbon materials for chemical capacitive energy storage, Adv. Mater. 23 (2011) 4828–4850.
[5] J. Wei, D. Zhou, Z. Sun, Y. Deng, Y. Xia, D. Zhao, A controllable synthesis of rich nitrogen-doped ordered mesoporous carbon for $CO_2$ capture and supercapacitors, Adv. Funct. Mater. 23 (2013) 2322–2328.
[6] Y. Fang, D. Gu, Y. Zou, Z. Wu, F. Li, R. Che, Y. Deng, B. Tu, D. Zhao, A low-concentration hydrothermal synthesis of biocompatible ordered mesoporous carbon nanospheres with tunable and uniform size, Angew. Chem. Int. Ed. 122 (2010) 8159–8163.
[7] R.J. White, K. Tauer, M. Antonietti, M.-M. Titirici, Functional hollow carbon nanospheres by latex templating, J. Am. Chem. Soc. 132 (2010) 17360–17363.
[8] J. Liu, T. Yang, D.-W. Wang, G.-Q. Lu, D. Zhao, S.-Z. Qiao, A facile soft-template synthesis of mesoporous polymeric and carbonaceous nanospheres, Nat. Commun. 4 (2013) 2798.
[9] J. Wei, Z.K. Sun, W. Luo, Y.H. Li, A.A. Elzatahry, A.M. Al-Enizi, Y. Deng, D. Zhao, New insight into the synthesis of large-pore ordered mesoporous materials, J. Am Chem. Soc. 139 (2017) 1706–1713.
[10] S. Wang, W.-C. Li, G.-P. Hao, Y. Hao, Q. Sun, X.-Q. Zhang, A.-H. Lu, Temperature-programmed precise control over the sizes of carbon nanospheres based on benzoxazine chemistry, J. Am. Chem. Soc. 133 (2011) 15304–15307.
[11] J. Li, Y. Liu, Z.-J. Zhu, G.-Z. Zhang, T. Zou, Z.-J. Zou, S. Zhang, D. Zeng, C. Xie, A full-sunlight-driven photocatalyst with super long-persistent energy storage ability, Sci. Rep. 3 (2013) 1430.
[12] J. Liu, S.-Z. Qiao, H. Liu, J. Chen, A. Orpe, D. Zhao, G. Lu, Extension of the Stöber method to the preparation of monodisperse resorcinol-formaldehyde resin polymer and carbon spheres, Angew. Chem. Int. Ed. 123 (2011) 6069–6073.
[13] J. Choma, D. Jamioła, K. Augustynek, M. Marszewski, M. Gao, M. Jaroniec, New opportunities in Stöber synthesis: preparation of microporous and mesoporous carbon spheres, J. Mater. Chem. 22 (2012) 12636–12642.
[14] Z.-A. Qiao, B. Guo, A.J. Binder, J. Chen, G.M. Veith, S. Dai, Controlled synthesis of mesoporous carbon nanostructures via a "Silica-Assisted" strategy, Nano Lett. 13 (2013) 207–212.
[15] X. Sun, Y. Li, Colloidal carbon spheres and their core/shell structures with noble-metal nanoparticles, Angew Chem. Int. Ed. 116 (2004) 607–611.
[16] Q. Wang, H. Li, L. Chen, X. Huang, Monodispersed hard carbon spherules with uniform nanopores, Carbon 39 (2001) 2211–2214.
[17] K. Ai, Y. Liu, C. Ruan, L. Lu, G. Lu, $Sp^2$ C-dominant N-doped carbon sub-micrometer spheres with a tunable size: aversatile platform for highly efficient oxygen-reduction catalysts, Adv. Mater. 25 (2013) 998–1003.
[18] J. Tang, J. Liu, C. Li, Y. Li, M.O. Tade, S. Dai, Y. Yamauchi, Synthesis of nitrogen-doped mesoporous carbon spheres with extra-large pores through assembly of diblock copolymer micelles, Angew. Chem. Int. Ed. 54 (2015) 588–593.
[19] S. Nizamuddin, H.A. Baloch, G.J. Griffin, N.M. Mubarak, A.W. Bhutto, R. Abro, S. A. Mazari, B.S. Ali, An overview of effect of process parameters on hydrothermal carbonization of biomass, Renew. Sust. Energ. Rev. 73 (2017) 1289–1299.
[20] J. Wang, P. Nie, B. Ding, S. Dong, X. Hao, H. Dou, X. Zhang, Biomass derived carbon for energy storage devices, J. Mater. Chem. A 5 (2017) 2411–2428.
[21] J. Deng, M. Li, Y. Wang, Biomass-derived carbon: synthesis and applications in energy storage and conversion, Green. Chem. 18 (2016) 4824–4854.
[22] M. Borghei, J. Lehtonen, L. Liu, O.J. Rojas, Advanced biomass-derived electrocatalysts for the oxygen reduction reaction, Adv. Mater. 30 (2018) 1703691.
[23] B. Hu, K. Wang, L. Wu, S.-H. Yu, M. Antonietti, M.-M. Titirici, Engineering carbon materials from the hydrothermal carbonization process of biomass, Adv. Mater. 22 (2010) 813–828.
[24] B. Zhu, B. Liu, C. Qu, H. Zhang, W. Guo, Z. Liang, F. Chen, R. Zou, Tailoring biomass-derived carbon for high-performance supercapacitors from controllably cultivated algae microspheres, J. Mater. Chem. A 6 (2018) 1523–1530.
[25] C. Wang, D. Wu, H. Wang, Z. Gao, F. Xu, K. Jiang, A green and scalable route to yield porous carbon sheets from biomass for supercapacitors with high capacity, J. Mater. Chem. A 6 (2018) 1244–1254.
[26] X. Wang, C. Zhan, Y. Ding, B. Ding, Y. Xu, S. Liu, D. Hua, Dual-core $Fe_2O_3$@Carbon structure derived from hydrothermal carbonization of chitosan as a highly efficient material for selective adsorption, ACS Sustain. Chem. Eng. 5 (2017) 1457–1467.
[27] Q.-L. Zhu, Q. Xu, Metal-organic framework composites, Chem. Soc. Rev. 43 (2014) 5468–5512.
[28] B. Liu, H. Shioyama, H. Jiang, X. Zhang, Q. Xu, Metal-organic framework (MOF) as a template for syntheses of nanoporous carbons as electrode materials for supercapacitor, Carbon 48 (2010) 456–463.
[29] W. Xia, A. Mahmood, R. Zou, Q. Xu, Metal-organic frameworks and their derived nanostructures for electrochemical energy storage and conversion, Energy. Environ. Sci. 8 (2015) 1837–1866.

[30] J. Wei, Y. Hu, Y. Liang, B. Kong, Z. Zheng, J. Zhang, S. Jiang, Y. Zhao, H. Wang, Graphene oxide/core–shell structured metal-organic framework nano-sandwiches and their derived cobalt/N-doped carbon nanosheets for oxygen reduction reactions, J. Mater. Chem. A 5 (2017) 10182–10189.
[31] J. Wei, Y. Hu, Y. Liang, B. Kong, J. Zhang, J. Song, Q. Bao, G.P. Simon, S. Jiang, H. Wang, Nitrogen-doped nanoporous carbon/graphene nano-sandwiches: synthesis and application for efficient oxygen reduction, Adv. Funct. Mater. 25 (2015) 5768–5777.
[32] X. Wang, J. Liu, S. Leong, X. Lin, J. Wei, B. Kong, Y. Xu, Z. Low, J. Yao, H. Wang, Rapid construction of ZnO@ZIF-8 heterostructures with size-selective photocatalysis properties, ACS Appl. Mater. Inter. 8 (2016) 9080–9087.
[33] H.-L. Jiang, B. Liu, Y.-Q. Lan, K. Kuratani, T. Akita, H. Shioyama, F. Zou, Q. Xu, From metal-organic framework to nanoporous carbon: toward a very high surface area and hydrogen uptake, J. Am. Chem. Soc. 133 (2011) 11854–11857.
[34] J. Wei, Y. Liang, Y. Hu, B. Kong, G.P. Simon, J. Zhang, S. Jiang, H. Wang, A versatile iron-tannin-framework ink coating strategy to fabricate biomass-derived iron carbide/Fe-N-carbon catalysts for efficient oxygen reduction, Angew. Chem. Int. Ed. 55 (2016) 1355–1359.
[35] M. Chen, Y. Zhang, L. Xing, Y. Liao, Y. Qiu, S. Yang, W. Li, Morphology-conserved transformations of metal-based precursors to hierarchically porous micro-/nanostructures for electrochemical energy conversion and storage, Adv. Mater. 29 (2017) 1607015.
[36] S.-J. Yang, M. Antonietti, N. Fechler, Self-assembly of metal phenolic mesocrystals and morphosynthetic transformation toward hierarchically porous carbons, J. Am. Chem. Soc. 137 (2015) 8269–8273.
[37] F.L. Braghiroli, V. Fierro, M.T. Izquierdo, J. Parmentier, A. Pizzi, A. Celzard, Nitrogen-doped carbon materials produced from hydrothermally treated tannin, Carbon 50 (2012) 5411–5420.
[38] A. Szczurek, V. Fierro, A. Pizzi, A. Celzard, Emulsion-templated porous carbon monoliths derived from tannins, Carbon 74 (2014) 352–362.
[39] S. Schlienger, A.-L. Graff, A. Celzard, J. Parmentier, Direct synthesis of ordered mesoporous polymer and carbon materials by a biosourced precursor, Green. Chem. 14 (2012) 313–316.
[40] C. Peter, A. Derible, J.-M. Becht, J. Kiener, C. Le Drian, J. Parmentier, V. Fierro, M. Girleanu, O. Ersen, Biosourced mesoporous carbon with embedded palladium nanoparticles by a one pot soft-template synthesis: application to Suzuki reactions, J. Mater. Chem. A 3 (2015) 12297–12306.
[41] F.L. Braghiroli, V. Fierro, J. Parmentier, A. Pasc, A. Celzard, Easy and eco-friendly synthesis of ordered mesoporous carbons by self-assembly of tannin with a block copolymer, Green. Chem. 18 (2016) 3265–3271.
[42] F.L. Braghiroli, V. Fierro, A. Szczurek, N. Stein, J. Parmentier, A. Celzard, Hydrothermally treated aminated tannin as precursor of N-doped carbon gels for supercapacitors, Carbon 90 (2015) 63–74.
[43] H. Ejima, J.J. Richardson, F. Caruso, Metal-phenolic networks as a versatile platform to engineer nanomaterials and biointerfaces, Nano Today 12 (2017) 136–148.
[44] H. Huang, J. Qin, G. Wang, Z. Guo, X. Yu, Y. Zhao, J. Wei, Synthesis of spiny metal-phenolic coordination crystals as a sensing platform for sequencespecific detection of nucleic acids, CrystEngComm 20 (2018) 7626–7630.
[45] J. Wei, Y. Liang, Y. Hu, B. Kong, J. Zhang, Q. Gu, Y. Dong, X. Wang, S. Jiang, H. Wang, Hydrothermal synthesis of metal-polyphenol coordination crystals and their derived metal/N-doped carbon composites for oxygen electrocatalysis, Angew. Chem. Int. Ed. 55 (2016) 12470–12474.
[46] P. Zhang, L. Wang, S. Yang, J.A. Schott, X. Liu, S.M. Mahurin, C. Huang, Y. Zhang, P.F. Fulvio, M.F. Chisholm, S. Dai, Solid-state synthesis of ordered mesoporous carbon catalysts via a mechanochemical assembly through coordination cross-linking, Nat. Commun. 8 (2017) 15020.
[47] J. Wei, G. Wang, F. Chen, M. Bai, Y. Liang, H. Wang, D. Zhao, Y. Zhao, Sol-gel synthesis of metal-phenolic coordination spheres and their derived carbon composites, Angew. Chem. Int. Ed. 130 (2018) 9986–9991.
[48] G. Wang, J. Qin, X. Zhou, Y. Deng, H. Wang, Y. Zhao, J. Wei, Self-template synthesis of mesoporous metal oxide spheres with metal-mediated inner architectures and superior sensing performance, Adv. Funct. Mater. 28 (2018) 1806144.
[49] A. Phan, C.J. Doonan, F.J. Uribe-Romo, C.B. Knobler, M. O'Keeffe, O.M. Yaghi, Synthesis, structure, and carbon dioxide capture properties of zeolitic imidazolate frameworks, Acc. Chem. Res. 43 (2010) 58–67.
[50] S. Morisada, Y.-H. Kim, T. Ogata, Y. Marutani, Y. Nakano, Improved adsorption behaviors of amine-modified tannin gel for palladium and platinum ions in acidic chloride solutions, Ind. Eng. Chem. Res. 50 (2011) 1875–1880.
[51] H. Zhang, H.-L. Zhang, A. Aldalbahi, X.-L. Zuo, C.-H. Fan, X.-Q. Mi, Fluorescent biosensors enabled by graphene and graphene oxide, Biosens. Bioelectron. 89 (2017) 96–106.
[52] N. Parvin, Q. Jin, Y. Wei, R. Yu, B. Zheng, L. Huang, Y. Zhang, L. Wang, H. Zhang, M. Gao, H. Zhao, W. Hu, Y. Li, D. Wang, Few-layer graphdiyne nanosheets applied for multiplexed real-time DNA detection, Adv. Mater. 29 (18) (2017) 1606755.
[53] F. Li, H. Pei, L. Wang, J. Lu, J. Gao, B. Jiang, X. Zhao, C. Fan, Nanomaterial-based fluorescent DNA analysis: acomparative study of the quenching effects of graphene oxide, carbon nanotubes, and gold nanoparticles, Adv. Funct. Mater. 23 (33) (2013) 4140–4148.
[54] H. Zhang, S. Jia, M. Lv, J. Shi, X. Zuo, S. Su, L. Wang, W. Huang, C. Fan, Q. Huang, Size-dependent programming of the dynamic range of graphene oxide-DNA interaction-based ion sensors, Anal. Chem. 86 (2014) 4047–4051.
[55] R. Rupaimoole, G.A. Calin, G. Lopez-Berestein, A.K. Sood, miRNA deregulation in cancer cells and the tumor microenvironment, Cancer. Discov. 6 (2016) 235–246.